Journal of Hydrology 635 (2024) 131171

Contents lists available at ScienceDirect

Journal of Hydrology

journal homepage: www.elsevier.com/locate/jhydrol

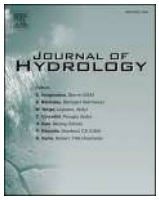

Research papers

Meltwater-driven sediment transport dynamics in two contrasting alpine proglacial streams

Michael Engel [a,2], Velio Coviello [a,1], Sara Savi [a,b,3], Anuschka Buter [a,4], Andrea Andreoli [a], Shusuke Miyata [a,c], Giulia Marchetti [a,5], Vittoria Scorpio [a,6], Sara Rathburn [d], Lindsey Nicholson [e], Francesco Comiti [a,f,*]

[a] Faculty of Agricultural, Environmental and Food Sciences, Free University of Bozen-Bolzano, Bolzano, Italy
[b] Institute for Geoscience, University of Potsdam, Germany
[c] Graduate School of Agriculture, Kyoto University, Japan
[d] Department of Geosciences, Colorado State University, USA
[e] Department of Atmospheric and Cryospheric Sciences, University of Innsbruck, Austria
[f] Dept. Land, Environment, Agriculture and Forestry, University of Padova, Italy

ARTICLE INFO

This manuscript was handled by Marco Borga, Editor-in-Chief, with the assistance of Edward Park, Associate Editor

Keywords:
Glacierized catchment
Sediment transport
Stable water isotopes
Tracer
Debris cover
Clean ice

ABSTRACT

Subglacial sediments are a large component of the sediment budget of glacierized catchments but insights into the subglacial origin of sediments (bedload, in particular) linked to proglacial runoff dynamics remain scarce. In this study, we use a tracer-based approach to quantify meltwater proportions related to sediment transport at two proglacial streams, draining glaciers (named debris-covered and clean glacier) of different size, aspect and elevation range with contrasting distribution and thickness of debris cover and lithology of the subglacial sediments (i.e., metamorphic vs. sedimentary), in the Sulden/Solda catchment (Italian Alps). Results indicate that the glacier melt component (75 to 80 %) was associated with bedload concentrations of 1 to 10 kg m^{-3} at the debris-covered glacier and much lower concentrations of 0.01 to 1 kg m^{-3} at the clean ice glacier. At the seasonal scale, bedload and suspended sediment concentrations at both sites strongly varied with discharge. While daily bedload concentrations varied by up to two orders of magnitude obscured the seasonal development of bedload concentrations at both sites, a clear seasonality for suspended sediment concentrations was found. At the daily scale, the relationship of discharge, bedload, and suspended sediment was more complex because discharge and sediment transport did not always follow the daily variation of air temperature, or similar daily air temperatures resulted in different discharge and sediment transport responses and vice versa. Glacier size, presence of debris cover, and substrate were identified as the main drivers of meltwater dynamics and sediment transport at both glaciers. This study adds further insights into the interplay of meltwater contributions and sediment transport, which are essential to better assess the impact of climate warming on sediment supply in glacierized catchments.

1. Introduction

Climate change strongly affects the cryosphere and modifies the runoff regime of glacierized and high-elevation catchments (Miller et al., 2012; Beniston and Stoffel, 2014; Gobiet et al., 2014). Increasing air temperatures and reduced snow cover in winter results in earlier and less pronounced snowmelt in spring and increased rates of ice melt from glaciers during summer (Beniston et al., 2018). At the decadal scale, several glacierized catchments have already surpassed their "peak water" stage of maximum annual discharge (Huss and Hock, 2018) or

* Corresponding author.
E-mail address: francesco.comiti@unipd.it (F. Comiti).
[1] Died in an accident on 1 April 2023.
[2] Now at: Federal Institute of Hydrology (BfG), Koblenz, Germany.
[3] Now at: Department of Earth and Environmental Sciences, University of Pavia, Italy.
[4] Now at: Hydronik GmbH, Emmerich am Rhein, Germany.
[5] Now at: Italian Institute for Environmental Protection and Research, Roma, Italy.
[6] Now at: Department of Chemical and Geological Sciences, University of Modena, Italy.

https://doi.org/10.1016/j.jhydrol.2024.131171
Received 10 December 2023; Received in revised form 26 March 2024; Accepted 28 March 2024
Available online 6 April 2024

approach it within the next decade (Duethmann et al., 2015) due to meltwater losses.

As a consequence of warming, glacier recession accelerates and the expansion of proglacial margins containing substantial unconsolidated debris accumulations may increase the amount of sediment available to fluvial transport and paraglacial reworking (Micheletti and Lane, 2016; Carrivick and Heckmann, 2017; Lane et al., 2017). High rates of rainfall, snowmelt, and glacier melt (Engel et al., 2016; Antoniazza et al., 2022) allow runoff events to reach a critical discharge threshold to initiate bed erosion and sediment entrainment, which ultimately determines the sediment transport in proglacial streams (Mao et al., 2017; Perolo et al., 2019). Such sediment transport, representing most of the overall catchment sediment yield (Heckmann and Schwanghart, 2013), originates from proglacial areas (such as frontal/lateral moraine or till-covered and steep valley sidewalls (Rabanser, 2019; Buter et al., 2020), subglacial till deposits (Perolo et al., 2019) and supraglacial/englacial sources (Fyffe et al., 2019b). Most of the sediment transport may continuously originate from subglacial till erosion (Delaney et al., 2018; Guillon et al., 2018).

In more detail, enhanced bedload transport results from the seasonal development of a subglacial drainage system within the ablation zone (Röthlisberger and Lang, 1987), which is responsible of subglacial erosion in late summer to autumn (Gurnell et al., 1996; Hallet et al., 1996; Delaney and Adhikari, 2020). As the melting season progresses, the dominant runoff contributions change from snowmelt to glacier melt (Penna et al., 2017) and the subglacial drainage system develops progressively from a distributed to a channelized system induced by strong daily melt cycles (Nienow et al., 1998), so that the evacuation of sediment below the glaciers increases over the course of the melting season (Swift et al., 2005). Such a seasonal development is controlled by the occurrences of high water-pressure events, hydro-meteorological conditions during the melting season, and the snow cover extent in early summer (Collins, 1989; Perolo et al., 2019). More specifically, high basal water pressure sets the base for the sensitivity of glacier melting for diurnal and seasonal variations (Cook and Swift, 2012).

In this context, the structure and seasonal evolution of the hydrological system may also depend on the glacier properties, as for example debris-covered glaciers and debris-free/clean glaciers, and differences in the timing and magnitude of proglacial runoff (Ayala et al., 2016; Fyffe et al., 2019b). The attenuating effect of the debris cover on the glacier ablation may lead to smaller input streams on the debris-covered area and a less efficient subglacial drainage system (Fyffe et al., 2019a), which in turn has implications for the subglacial sediment transport and proglacial hydrochemistry.

The evolution of such meltwater pathways indicates the complex behaviour of the glacial system, expressing the need for a better understanding of sediment availability and contribution (Haritashya et al., 2006). Despite the need for more insights into subglacial sediment sources (Delaney et al., 2018), most research has emphasized fine sediments (e.g., Collins, 1989; Hasnain and Thayyen, 1999; Swift et al., 2005; Haritashya et al., 2006) with few studies focused on bedload (Mao et al., 2019). Bedload dynamics of proglacial streams were often investigated a few kilometers downstream from the glacier (Pearce et al., 2003; Mao et al., 2014; Carrillo and Mao, 2020) and thus cannot be linked to subglacial sediment sources (Comiti et al., 2019). Indeed, bedload dynamics at the glacier snout may likely differ from those further downstream and thus represent a way to characterize the sediment supply system from the glacier (Pearce et al., 2003; Mao et al., 2014).

In this study, we used a tracer-based approach to quantify meltwater proportions linked to bedload transport measured at two proglacial streams (period 2017–2019), draining two glaciers that contrast in terms of size, presence and thickness of debris cover, lithology of the subglacial sediments (i.e., metamorphic vs. sedimentary), aspect and elevation range in the Sulden/Solda catchment (Italian Alps). Our study aim is to test the hypothesis that these contrasting features determine different runoff dynamics and subsequently contrasting sediment transport at the proglacial streams.

The study builds on the previous work of Comiti et al. (2019), who related bedload transport to estimates of glacier melt from the nearby Matsch/Mazia glacier. It further complements the recent insights into the study area on the subglacial drainage area (Ronald, 2020), the sedimentology of the lateral moraines (Rabanser, 2019) and the reconstruction of the past glacier extents (Savi et al., 2021b). Additional research has focused on river hydrochemistry (Engel et al., 2018), sediment transport (Coviello et al., 2022) and sediment connectivity (Buter et al., 2022; Savi et al., 2023) at the catchment scale.

In this regard, the objectives of the present study are:

- to hydrochemically identify the dominant meltwater (snowmelt vs. glacier melt) component at two proglacial streams,
- to analyse the temporal and spatial variability of meltwater and sediment transport, and
- to assess the sensitivity of meteorological conditions and runoff components on sediment transport.

2. Material and methods

2.1. Study area

The study area is the upper portion (14.8 km^2 in area) of the Sulden / Solda river basin (overall 130 km^2, eastern Italian Alps). The elevation of the analysed catchment ranges from 2225 m a.s.l. to the 3896 m a.s.l. of the Ortler/Ortles peak. The Sulden valley is mainly underlain by sedimentary (dolomitic) and volcanic (intrusions) rocks in the south-western part, and by metamorphic (mica-gneiss and schist) rocks in the south-eastern part of the catchment (Buter et al., 2020; Savi et al., 2021). Continuous permafrost is located above 2600 m a.s.l., (Boeckli et al., 2012), with active rock glaciers present between 2400 and 2900 m a.s.l. (Brighenti et al., 2019). In the Sulden basin, vegetation covers about 35 % of the total catchment area, with the coniferous tree line near 2000 m a.s.l. (Buter et al., 2020). The long-term mean annual air temperature at the Sulden village station is 2.8 °C and −2.4 °C at the Madritsch station (reference period: 1981–2010; 3PClim database; https://www.3pclim.eu/), with mean annual precipitation of 835 mm and 980 mm for Sulden and Madritsch, respectively. Both nivo-meteorological conditions and sub-catchment geology have a strong impact on meltwaters contributions and thus runoff dynamics and stream hydrochemistry in the catchment (Engel et al., 2018). Glacier melt and storm-induced high flows are the major drivers of sediment transport at the valley outlet (Coviello et al., 2022).

The formerly larger Sulden glacier fragmented after the 1950s into two ice bodies (Savi et al., 2021b), called Sulden I and Sulden glaciers. Over the last decades, the ice loss was substantial and at 0.7 ± 0.08 m w. e. a^{-1} (1985–2020) for the Sulden Glacier (Savi et al., 2021b) and 0.9 w. e. a^{-1} (2003–2013) for the wider Ortler-Cevedale Group (Galos et al., 2015). The sampling sites selected for this study were located at the proglacial streams draining the eastern part of the clean-ice Sulden I glacier (hereinafter CG) and the eastern part of the debris-covered Sulden glacier (hereinafter DG; Central Sulden in Savi et al., 2021b) (Fig. 1). Both glaciers differ in their extent, subglacial bedrock type, presence of debris-cover, and supraglacial streams (Table 1). Since the latest advance in 1986, the CG has been melting more rapidly and spatially uniformly than the DG, which primarily lost ice mass by glacier thinning rather than by frontal retreat (Savi et al., 2021b).

2.2. Instrumentation and field sampling

Meteorological data were provided by the automatic weather station (AWS) Madritsch / Madriccio (located at 2825 m a.s.l. and maintained by the Hydrographic Office of the Autonomous Province of Bozen-Bolzano). A pressure transducer was installed in the Sulden River

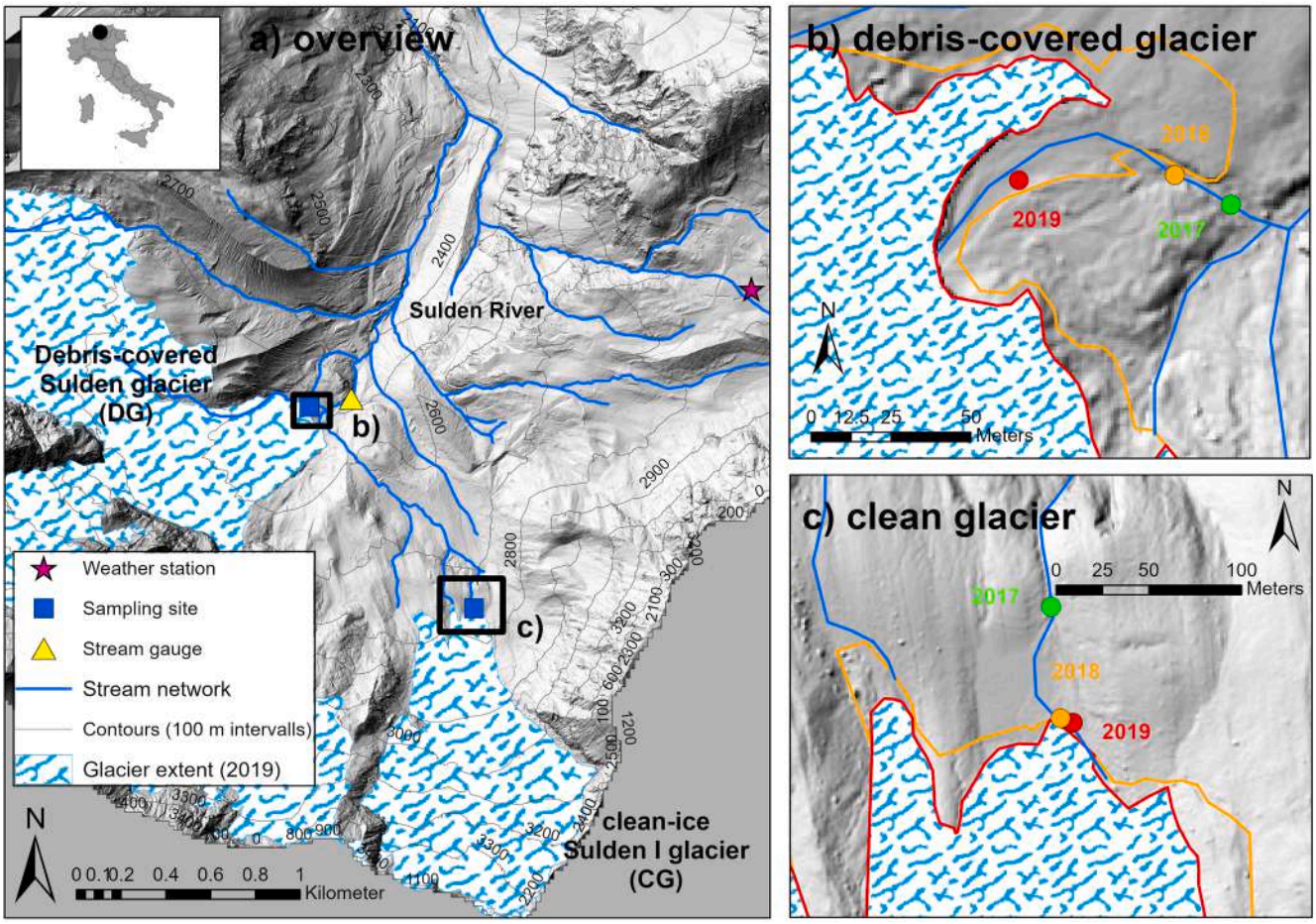

Fig. 1. Overview of the debris-covered (DG) and clean ice (CG) glacier sampling locations in the Upper Sulden catchment and the glacier extents of the previous years for both sampling sites. The different colours in subplot b and c) mark the different years and its corresponding glacier extent and sampling site.

Table 1
Glacio-geomorphological characteristics of the Sulden I glacier (CG) and the Sulden glacier (DG).

	CG (Sulden I glacier)	DG (Sulden glacier)
Glacier extent in 2018 (km^2)*	0.87	3.89
Glacier extent in 2019 (km^2) (loss in % compared to the previous year)*	0.83 (-4.6 %)	3.81 (-2%)
Elevation range (in 2019)	2732–3366	2481–3698
Mean elevation (m a.s.l.)	3035	2916
Mean slope (°)	28°	23°
Mean aspect	352° (Northwest)	122° (Southeast)
Supraglacial features	Small supraglacial streams and very limited debris cover	Debris cover of variable thickness (1–67 cm**)
Bedrock type	Metamorphic rocks	Metamorphic rocks, Conglomerates of metamorphic and sedimentary rocks
Debris type	Very few metamorphic from sporadic rock falls	Mostly dolomitic and metamorphic

* The extent was delineated from orthofotos taken in 2018 and 2019 (Autonomous Province of Bozen-Bolzano).
** data derived from 380 pits dug in August 2015 and 2018 (Nicholson and Boxall, 2020).

(Fig. 1a), which continuously recorded water stage at 10-minute measurement intervals from May to September/October 2017 to 2019 (Fig. 1). Because the river banks were unstable and eroded in places, we had to adjust the stream gauge position at the monthly and yearly scale and obtain new flow rating curves for each position.

Direct bedload sampling was carried out at CG (n = 34) and DG (n = 66) sites from June to September 2017 to 2019, by following a concurrent sampling approach at both sites (Fig. 1b, c and Fig. 2). "Bunte" bedload traps (4 mm mesh size, 20 × 30 cm opening, Bunte et al., 2004) were preferably placed at the thalweg, more precisely at a single position (stream width: 0.8–3.5 m) at CG and mostly at two positions (stream width: 2.3–7 m) at DG, accounting for the flow of different stream branches when the subglacial outflow was divided. For many days during the melting season, we repeated the sampling procedure during melt-induced runoff events to obtain daily hydro-sedimentary variations (from 10:00 to 17:00). Sampling durations ranged from 5 to 15 min and 1 to 10 min at CG and DG, respectively.

For each bedload sampling, we measured water stage and then estimated discharge using stage-discharge relationships based on salt dilution discharge measurements. Measured discharges ranged from 0.04 to 0.74 m^3/s at CG and 0.27 to 2.65 m^3/s at DG. Each bedload sampling event was accompanied by grab sampling of suspended sediment (into 0.5 l PVC bottles) (CG: n = 34 and DG: n = 66) and water sampling for tracer measurements of EC and stable water isotopes δ^2H and $\delta^{18}O$ (into 50 ml PVC bottles with double cap and no headspace). To identify potential end-members for runoff (i.e., snowmelt versus glacier melt), water sampling focused on ice melt from rivulets on the glacier surface at CG and dripping ice fragments at DG (called "glacier melt"),

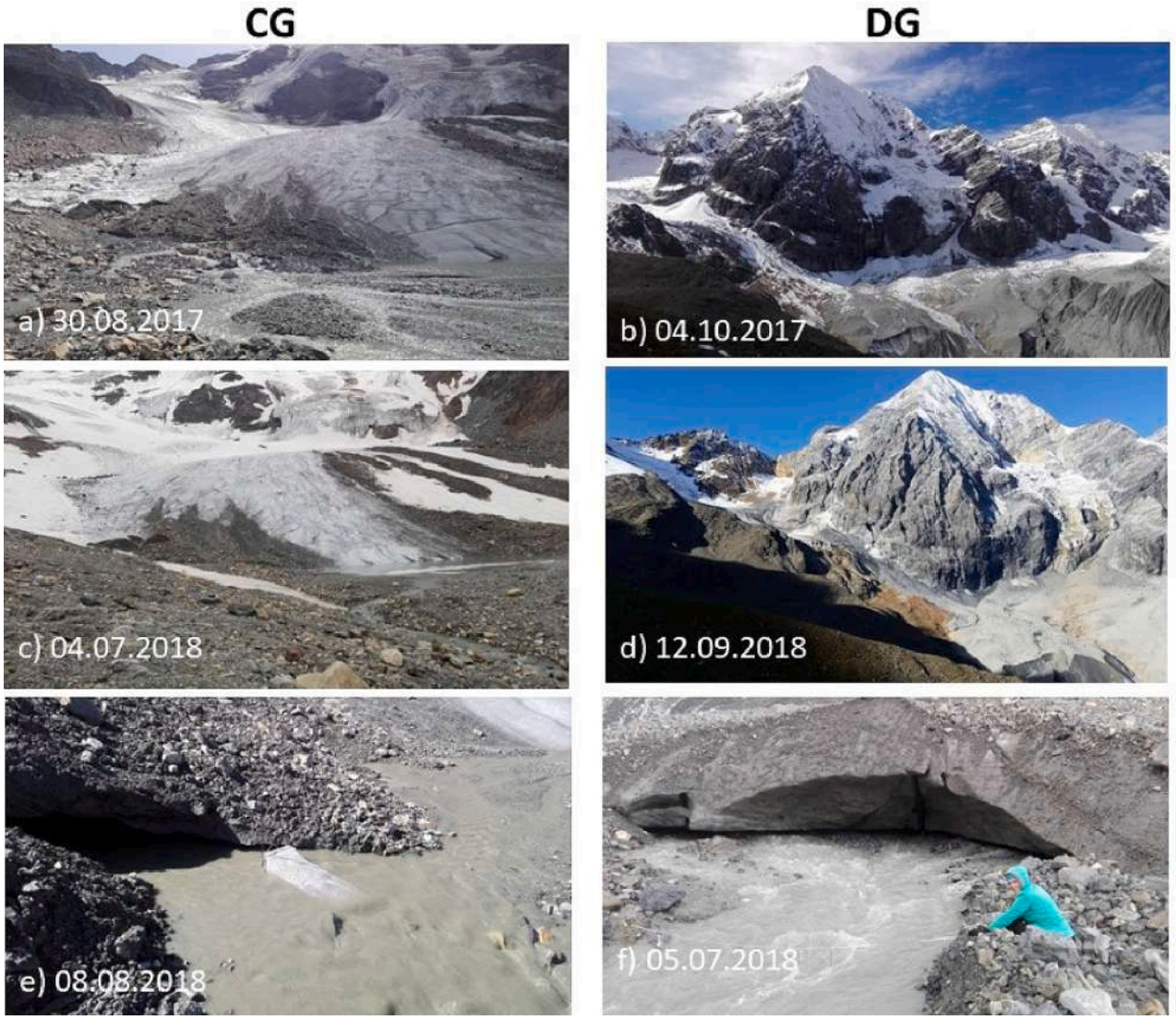

Fig. 2. Overview of the proglacial area and the sampling location at CG and DG for the years 2017 to 2018. Subplot e) shows the Bunte trap sampling at CG, and subplot f) shows a cross section measurement at DG.

which we performed after each bedload sampling. We sampled snowmelt from dripping snow patches in the area to capture the spatial variability of snowmelt (called "snowmelt"). The proglacial stream at CG and DG was sampled after each bedload sampling and once (not accompanied with sediment sampling) in January 2020 at DG (called "proglacial stream"). To infer the role of precipitation on runoff formation, we furthermore collected monthly precipitation near the mountain hut Schaubach at 2581 m asl. (n = 11, using a PALMEX collector, Gröning et al., 2012) and also sampled rain from a few occasional storms within the study area (n = 8).

2.3. Laboratory analysis

Bedload samples were dried at 65 °C, sieved and weighed. The grain size distributions D10, D30, D50, and D90 were calculated (i.e. quantiles, diameters Dx for which x% of the sampled sediment is finer). In the following, sediment transport is reported as bedload concentration, unit bedload rates, and unit stream power (Comiti et al., 2019). The total and unit bedload transport rates for the entire cross-section (Q_S in kg min^{-1} and q_S in kg m^{-1} s^{-1}, respectively) were estimated as width-weighted averages based on the sampling positions (see Dell'Agnese et al., 2014). Bedload concentration (in kg m^{-3}) was calculated by dividing total bedload rate by measured discharge.

Unit stream power ω (in W m^{-2}) was calculated for each bedload sample from CG and DG as follows (Eq. (1)):

$$\omega = \gamma \, Q \, S/W$$

where γ is the specific weight of water (assumed constant and equal to 9810 N m^{-3}), Q is the water discharge (m^3/s), S is the channel slope (mm^{-1}), and W is the channel width (m).

Suspended sediment concentration (SSC hereafter) samples were filtered by vacuum filtration by using a Millipore filtration system (with non-nitrate Whatman filter, ∅ 0.45 μm) in the laboratories of the Free University of Bozen-Bolzano. The samples were dried in the oven at 105 °C for an hour and cooled in the desiccator for 30 min.

Stable water isotope samples were first stored in a dark fridge at 4 °C and then the δ^2H and $\delta^{18}O$ isotopic composition was measured by laser spectroscopy (L2130-i, Picarro Inc., USA) at the Free University of Bozen-Bolzano. The instrumental precision is 0.5 ‰ for δ^2H and 0.25 ‰ for $\delta^{18}O$. EC was measured using a portable WTW 3410 conductivity meter (WTW GmbH, Germany), which has a precision of ±0.1 μS cm^{-1} (nonlinearly corrected by temperature compensation at 25 °C).

2.4. Data analysis

To estimate glacier melt fractions, we calculated the runoff components during each bedload sampling using a two-component hydrograph separation based on end-member mixing (Klaus and McDonnell, 2013). The following assumptions related to the definitions of the event (snowmelt or glacier melt during bedload sampling) and pre-event (proglacial stream water with highest solute concentration during low flow conditions) were made: i) the tracer concentration of the event contributions are distinct from that of the pre-event; (2) stream discharge can be approximated as a mixture of the two components; and (3) the tracer composition of each component can be assumed to be constant during the event or is known from measurements (Sklash and Farvolden, 1979). Although this method is known to have limitations with respect to the different information content tracers carry in hydrograph separation or the behavior of solute tracer to be sometimes non-conservative (Christopherson and Hooper, 1992), numerous studies highlight their usefullness. Therefore, to minimize methodological uncertainties, we used EC over isotopic composition as this tracer exhibited the largest difference in concentration for the meltwater and stream component (Genereux, 1998) and we further relied on hydrochemical data from meltwater samples taken immediately after each bedload sampling.

For CG, we defined the following mass balance Eq. (2):

$$F_{GlaciermeltCG} = \frac{EC_{CG} - EC_{MAX}}{EC_{GM} - EC_{MAX}} \quad (2)$$

where F is the fraction of the glacier melt from total runoff, *EC* denotes the electrical conductivity from the proglacial stream CG, the glacier melt *GM* from clean-ice near the sampling site CG, and *MAX* denotes the proglacial stream at the end of August 2018, when measured EC was highest.

For DG, we defined the following mass balance equation (Eq. (3)) analogous to Eq. (2):

$$F_{GlaciermeltDG} = \frac{EC_{DG} - EC_{MAX}}{EC_{GM} - EC_{MAX}} \quad (3)$$

where F is the fraction of the glacier melt from total runoff, *EC* denotes the electrical conductivity from the proglacial stream DG, the glacier melt *GM* from debris-covered glacier ice near the sampling site DG, and *MAX* denotes the proglacial stream in January 2020, when highest EC was measured during winter low flow conditions. The exploration of stable water isotopes as tracer at CG and DG did not obtain reliable results and was not considered further.

Instead, a three-component hydrograph separation was applied for end-member mixing at DG on 24.07.2019. The assumptions previously written are valid here as well and extended to snowmelt and glacier melt as event water components. Therefore, we defined the mass balance equation as follows (Eq. (4) – Eq. (6)):

$$F_{lowflow} = \frac{(\delta_T - \delta_{GM})x(EC_S - EC_{GM}) - (\delta_S - \delta_{GM})x(EC_T - EC_{GM})}{(\delta_{GR} - \delta_{GM})x(EC_S - EC_{GM}) - (\delta_S - \delta_{GM})x(EC_{GR} - EC_{GM})} \quad (4)$$

$$F_{snowmelt} = \frac{(\delta_T - \delta_{GM})x(EC_{GR} - EC_{GM}) - (\delta_{GR} - \delta_{GM})x(EC_T - EC_{GM})}{(\delta_S - \delta_{GM})x(EC_{GR} - EC_{GM}) - (\delta_{GR} - \delta_{GM})x(EC_S - EC_{GM})} \quad (5)$$

$$F_{glaciermelt} = F_{total} - F_{lowflow} - F_{snowmelt} \quad (6)$$

where δ indicates the isotopic composition ($\delta^{18}O$) and EC denotes the electrical conductivity. F denotes the discharge fraction of the low flow component (*low flow*), snowmelt (*snow melt*), glacier melt (*glacier melt*), and total runoff (*total*) at DG on 24.07.2019.

For statistical analysis, we used the Kolmogorov-Smirnov test to verify the normal distribution of the data. In the case of non-normally distributed data, we applied the non-parametric Wilcoxon rank sum test to compare different sample groups on their significant difference (significance level $\alpha = 0.01$).

3. Results

3.1. Tracer-based characterisation of the proglacial runoff generation

Using $\delta^{18}O$ and EC to characterize the hydrochemistry of the proglacial streams CG and DG, the hydrochemical mixing space was defined by four end-members: snowmelt, glacier melt, a water component rich in solutes, and monthly precipitation. While the mixing of snowmelt and glacier melt with water rich in solutes could mainly explain the hydrochemistry at CG and DG, both monthly precipitation and occasional rain events did not affect the hydrochemistry and thus did not contribute to runoff generation during sampling days (Fig. 3).

Generally, the mixing space of both locations overlapped well and showed relatively similar hydrochemical characteristics for the end-members (Table 2). However, differences were observed in the range of EC for glacier melt ($\rho < 0.001$) and the proglacial streams ($\rho < 0.001$) but not for snowmelt ($\rho = 0.26$). Particularly at DG, we identified a water component with increased EC (1006 µS cm^{-1}, represented by winter baseflow proglacial stream water) and similar isotopic composition compared to that from glacier melt ($\delta^{18}O$: −14.82 ‰). An isotopic fractionation altering the $\delta^{18}O$ composition was not observed (Fig. S1). However, the isotopic composition of glacier melt (CG: $\rho = 0.003$ and $\rho < 0.001$; DG: $\rho = 0.001$ and $\rho < 0.001$) and proglacial stream water (CG: $\rho = 0.008$ and $\rho < 0.001$; DG: $\rho = 0.005$ and $\rho < 0.001$) showed mainly variations for the years 2018 and 2019, respectively (Fig. S2).

3.2. Temporal and spatial variability of sediment transport

Meteorological characteristics are summarized in Table 3 and showed that 2018 and 2019 summers were generally drier (total precipitation: 461 – 497 mm) and warmer (about 87 days with median air temperature > 5 °C) than in 2017. Discharge variations of the proglacial stream at the stream gauge location strongly followed the dynamics of air temperature and rain events (Fig. 4). High flows higher than 4 m^3/s were present every year and reached a maximum of about 7 m^3/s (at the beginning of August 2017), associated with a particularly warm period of a few days with a maximum daily mean air temperature of 14 °C at 2825 m asl. Discharges below 1 m^3/s characterized the low flows, which were typically initiated by cooler days in late summer and autumn with air temperatures dropping below 0 °C (for example, clearly visible at the beginning of September 2017).

Seasonal bedload concentrations and SSC at CG and DG varied similarly with discharge (Fig. 4). SSC at both sites showed a clear seasonality, with larger monthly variations of three orders of magnitude at DG and only one order of magnitude at CG. In contrast, the seasonal development of bedload concentrations at CG and DG was less clear as bedload concentrations were characterized by large daily variations of up to two orders of magnitude. For example, during high flows of about 2.6 m^3/s at the end of August 2018, the highest bedload concentrations of more than 1 kg m^{-3} and SSC of about 12 g l^{-1} at DG were measured. During the same period, bedload concentrations at CG were two orders of magnitude lower than at DG. Instead, SSC reached about 9 g l^{-1} and was thus similar to SSC at DG. Interestingly, observed daily minima of bedload concentration and SSC in June and July were similar to those towards the end of the melting season in September.

At the daily scale, increasing discharge induced by rising air temperatures during the day generally controlled the dynamics of bedload and SSC (Fig.5). The time of daily air temperature peaks generally matched the time when the maximum discharge and sediment transport was reached, for example, on 10 July 2019 at DG and 24 July 2019 at CG and 22 Aug 2018 at CG and DG. The intra-daily variability at DG was persistently about one order of magnitude for bedload rates and SSC from June to August.

In contrast to this previous observation, the dynamics of bedload and

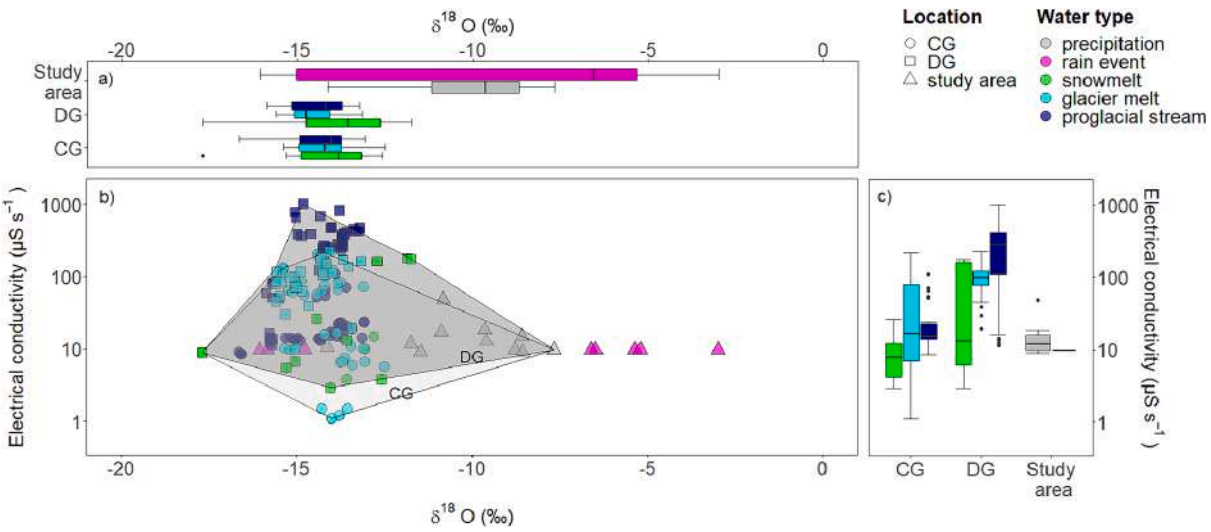

Fig. 3. a) Boxplots $\delta^{18}O$ for different water types sampled from 2017 to 2019. b) Bi-plot based on $\delta^{18}O$ and electrical conductivity indicating the tracer mixing space of CG and DG. c) Boxplots of electrical conductivity for different water types sampled from 2017 to 2019. The study area refers to the periglacial areas of CG and DG.

Table 2
Tracer-based summary of statistical characteristics of the end-member hydrochemistry. Monthly precipitation does not include rain events, which were occasionally sampled.

End-member	Number of samples	$\delta^{18}O$ (‰)			EC (µS cm^{-1})			Location
		Mean	SD	Range	Mean	SD	Range	
Monthly precipitation	11	−10.1	1.8	−14.1 to −7.6	15.6	11.4	9 to 48.5	Study area
Snowmelt	10	−14.2	1.5	−17.7 to −12.6	9.5	7.0	2.9 to 26	CG
Glacier melt	35	−14.2	0.7	−15.4 to −12.5	53.5	60.0	1.1 to 214	
Proglacial stream	35	−14.4	1.0	−16.6 to − 13.0	23.7	21.5	8.5 to 111.5	
Snowmelt	11	−13.8	1.7	−17.7 to −11.7	67.7	81.1	2.9 to 178.2	DG
Glacier melt	34	−14.6	0.7	−15.6 to −13.1	103.5	46.5	19.4 to 224	
Proglacial stream	44	−14.4	0.8	−15.9 to −13.2	312	234	11.4 to 1006	

Table 3
Meteorological characteristics of the study area summarized for the period 1st of June to 1st of October from 2017 to 2019. Data were taken from AWS Madritsch.

Meteorological parameter	2017	2018	2019
Total precipitation (mm)	554	461	497
Number of days with total precipitation > 10 (mm d^{-1})	21	17	19
Median air temperature (°C)	6.13	6.18	6.47
Number of days with median air temperature > 5 (°C)	68	88	87
Number of days with median air temperature > 10 (°C)	18	9	17
Days with snow depth increase by 5 cm	6	2	3

SSC at the daily scale were more complex and non-linear as i) discharge and sediment transport did not always follow the daily variation of air temperature by a clear rising and falling limb, ii) at CG, relatively constant discharges of about 0.1 l s^{-1} were accompanied with variable sediment transport on 27 June, 10 and 24 July 2019, and iii) similar daily air temperatures resulted in different discharge and sediment transport responses and vice versa. For example, similar daily air temperatures on 27 June and 24 July 2019 led to higher discharge and sediment transport in July compared to June at CG and DG. In turn, although air temperature on 10 July and 24 July 2019 differed by about 9 °C, discharge and sediment transport were at similar orders of magnitude at both sites. In contrast, relatively similar air temperatures on 8 and 22 Aug 2018 led to discharges of 0.85 m^3/s at DG, unit bedload rates of 0.2 kg s^{-1} m^{-1}, and SSC of 10.8 g l^{-1} during the first date, but showed an increased discharge of about 1.4 m^3/s, one order of magnitude higher unit bedload rates, and one order of magnitude lower SSC two weeks later.

To compare unit bedload rates and SSC for different hydrological conditions at CG and DG, we show these parameters related to the unit stream power (Fig. 6). Unit bedload rates at CG were much lower than those at DG ($\rho < 0.001$) and ranged from 22.3 to 341 W m^{-2} with no clear monthly variation (Fig. 6a, 6b). Unit bedload rates and SSC were lower in June and July (mean q_S: 0.0028 kg s^{-1} m^{-1}; mean SSC: 0.39 g l^{-1}, respectively) and by up to two orders of magnitude higher in August (mean q_S: 0.023 kg s^{-1} m^{-1}; mean SSC: 1.8 g l^{-1}, respectively). At DG, unit stream power had a much wider range (74 to 581 W m^{-2}), with higher values associated to increased unit bedload rates and SSC in July and August; while unit bedload rates below 0.001 kg s^{-1} m^{-1} were observed during low flows of 100 W m^{-2} in September, they were almost four orders of magnitude higher when unit stream powers reached 200 – 300 W m^{-2} in July and August (for few samples also in June, Fig. 6b). Similarly, lowest SSC was measured in September (mean: 0.16 g l^{-1}) but increased by two orders of magnitude to reach a maximum of 11.8 g l^{-1} in July and August. In particular, the unit stream power – SSC data could be roughly approximated by a logarithmic relationship, indicating an SSC threshold at around 10 g l^{-1} for varying unit stream power (Fig. 6d).

Furthermore, to better characterize the sediment supply at CG and DG, daily hysteresis of bedload concentration and SSC against discharge, snowmelt, and glacier melt proportion is shown (Figs. 7 and 8). While the majority of analysed events did not show clear hysteresis, only some events showed a clockwise pattern when the peak of bedload concentration or SSC occurred before the peak of discharge and meltwater. Instead, on days with counterclockwise hysteresis, the peak of bedload concentration or SSC occurred after the peak of discharge and meltwater (Table 4). No clear hysteresis pattern of discharge and meltwater compared with the locations, or season was evident (Table 4).

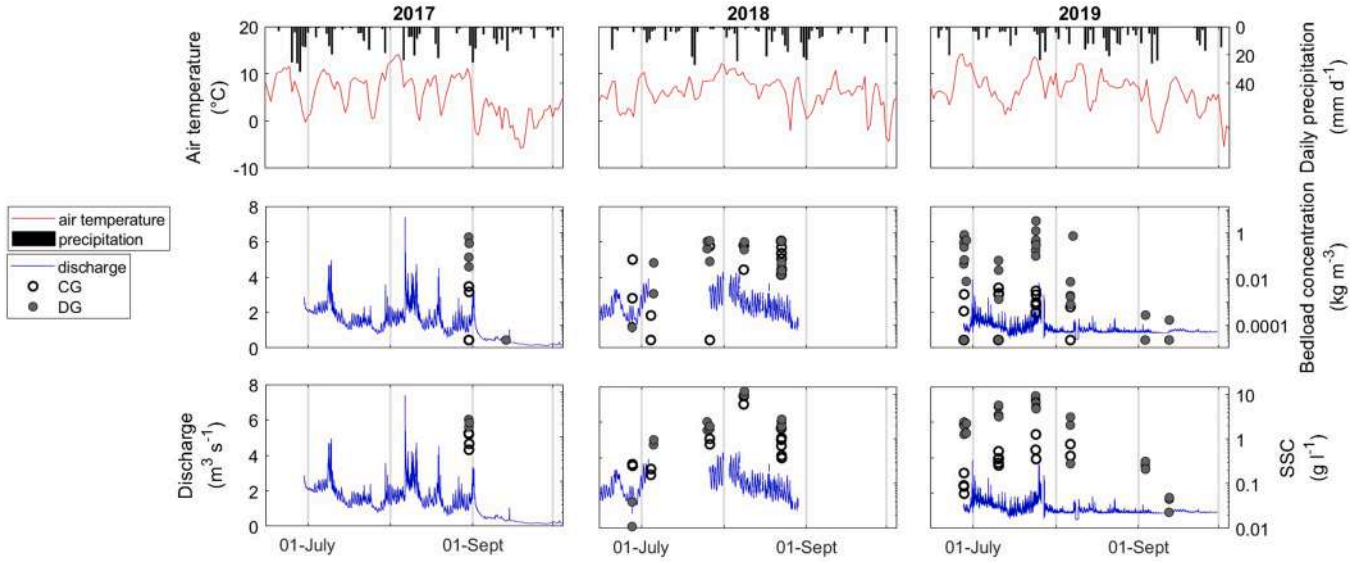

Fig. 4. Variations of meteorological and hydrological conditions combined with bedload concentration and SSC at the sampling sites CG and DG from 2017 to 2019. Discharge was calculated from water stages measured at the stream gauge. Water stages in 2019 were corrected following Arnoldi (2021). Meteorological parameters were measured at AWS Madritsch.

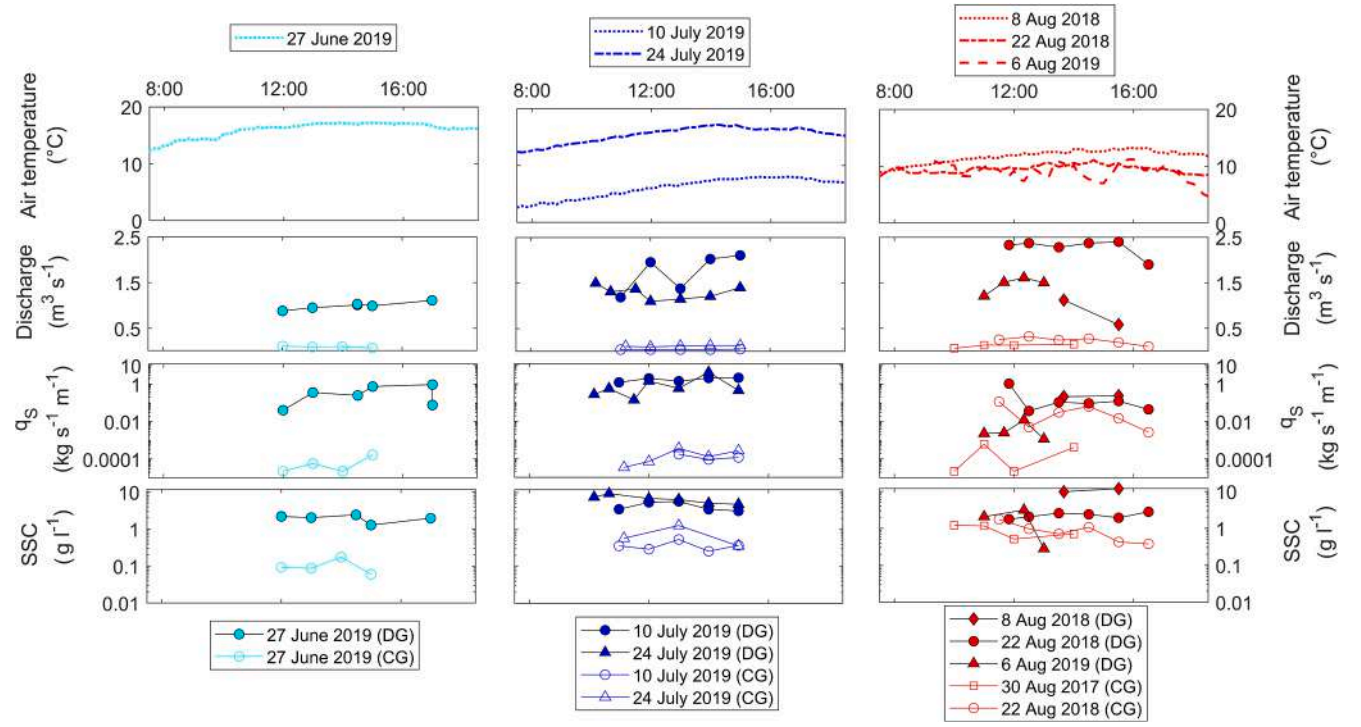

Fig. 5. Monthly variations of air temperature (upper row), discharge (second row), unit bedload rate (third row), and SSC (last row) at CG and DG for selected days in June, July, and August from 2017 to 2019 in the Upper Sulden catchment.

3.3. Impact of meteorological conditions and runoff components on sediment fluxes

Bedload concentrations at both proglacial streams were clearly controlled by glacier melt and slightly by the presence of snowmelt (Fig. 9). First, the relationship between glacier melt fraction and bedload concentration revealed relatively low bedload concentrations of up to 0.001 kg m^{-3} during low to medium glacier melt contribution (19 to 58 %) at CG and DG in June (Fig. 9b). In contrast, higher glacier melt contributions were associated with larger variability in bedload concentrations. Glacier melt of 75 to 80 % resulted in bedload concentrations of 1 to 10 kg m^{-3} at DG but in much lower concentrations of 0.01 to 1 kg m^{-3} at CG. When glacier melt at DG was absent, snowmelt as dominant runoff component led to similar bedload concentrations than observed during highest glacier melt. Moreover, DG samples from 2018 did not show a monthly variability, leading to a cluster at high glacier melt conditions with 0.1 to 1 kg m^{-3} of bedload concentration.

Hydro-meteorological conditions indicated that highest glacier melt occurred when the 3-day mean air temperature was above 10 °C and only little precipitation fell (Fig. 9c and d).

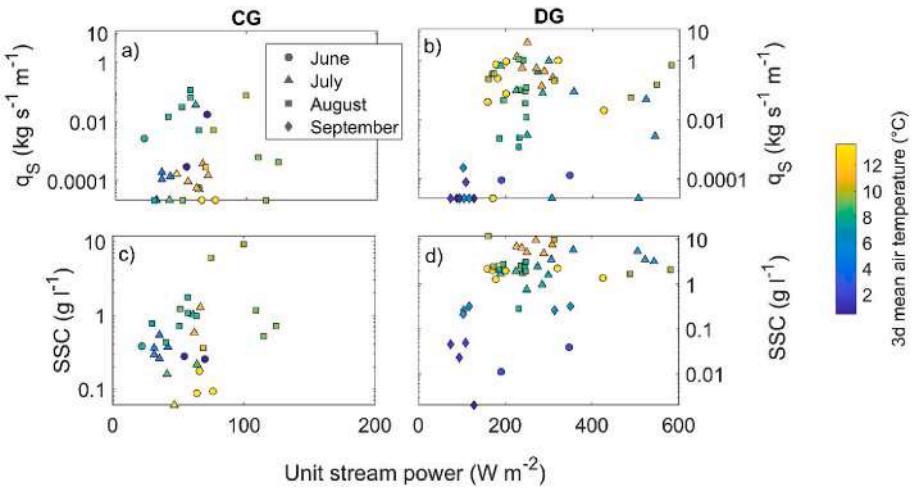

Fig. 6. Monthly variations of (a, b) unit bedload rates (per unit of channel width) and of (c, d) suspended sediment concentration (SSC) shown against unt stream power measured at CG and DG in the Upper Sulden catchment. The color codes the 3-day mean air temperature at AWS Madritsch. Note the different scale of unit stream power on the x-axis on the left and right subplots.

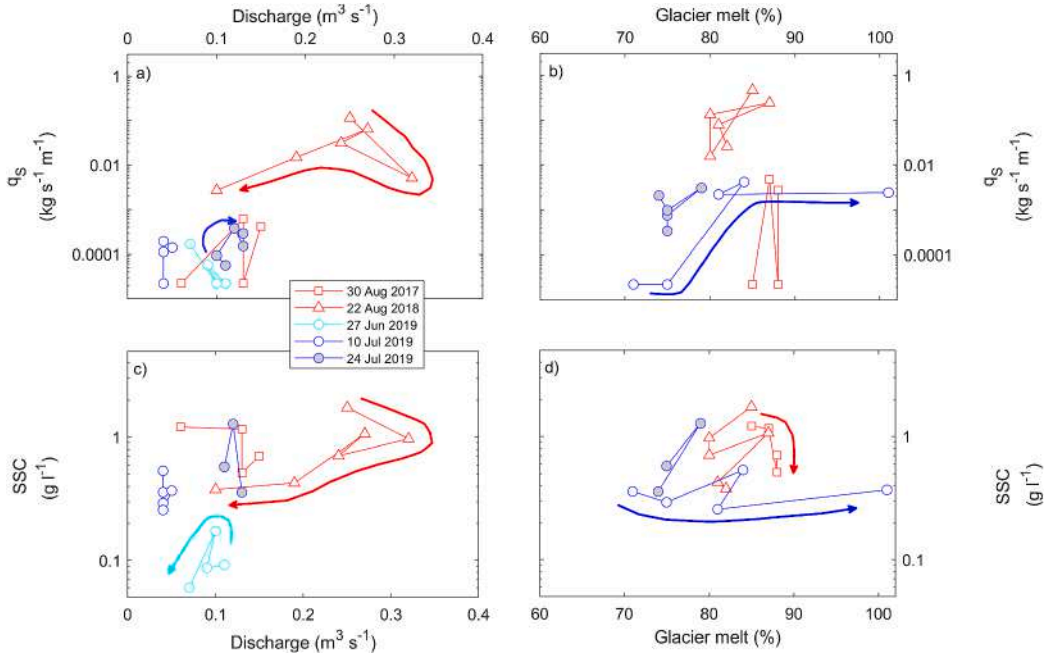

Fig. 7. Hysteresis of discharge, meltwater proportion (glacier melt in %), bedload concentration, and SSC at CG on sampling days from 2017 to 2019.

Surprisingly, highest discharges were not composed of only glacier melt but shared also minor proportions of snowmelt of up to 25 % (Fig. 9e). While the proportions of snowmelt did not seem to have much effect on EC at CG, increasing glacier melt proportions led to markedly decreasing EC at DG (Fig. 9f). The variability of bedload concentration during the snowmelt period in June revealed similar orders of magnitude than those during the glacier melt period.

3.4. *Variability of grain size distributions*

Sediment samples from CG and DG were significantly different with respect to grain size distributions of D10, D30, D50, and D90 ($\rho = 0.004$, $\rho < 0.001$, $\rho < 0.001$, $\rho < 0.001$, respectively), for which grain sizes were 2.1 mm, 3.9 mm, 4.1 mm, and 8.5 mm at CG and 3.0 mm, 5.9 mm, 10.6 mm, and 27.4 mm at DG (Fig. 10a). These differences in grain size distribution are supported by field observation indicating that bedload from DG mostly consisted of dolomitic rocks with a share of conglomerates, while bedload from CG was only metamorphic.

By analysing the grain size distributions only for bedload samples taken when snowmelt or glacier melt contribution was greater than 60 %, the grain size distribution was not significantly different with respect to the major runoff component (CG: $\rho = 0.11 < 0.32$; DG: $\rho = 0.06 < 0.95$). At DG, there was the tendency for larger sediments (32 mm) to be more often associated with glacier melt than snowmelt (22 mm) when considering D90 (Fig. 10c).

When comparing unit stream power with grain sizes, increasing unit stream power resulted in increasing grain sizes for all distributions at both sites (Fig. 11a and b). Also increasing glacier melt resulted in larger grain sizes at CG and DG (Fig. 11c and d), similar to the previous observation at DG (Fig. 10c). During the absence of glacier melt, the range of grain sizes at CG (0 to 19.7 mm) was similar to that during glacier melt (0 to 21.4 mm). In contrast, this range was much wider at DG during glacier melt (0 to 86 mm) than that during snowmelt only (0 to 43 mm).

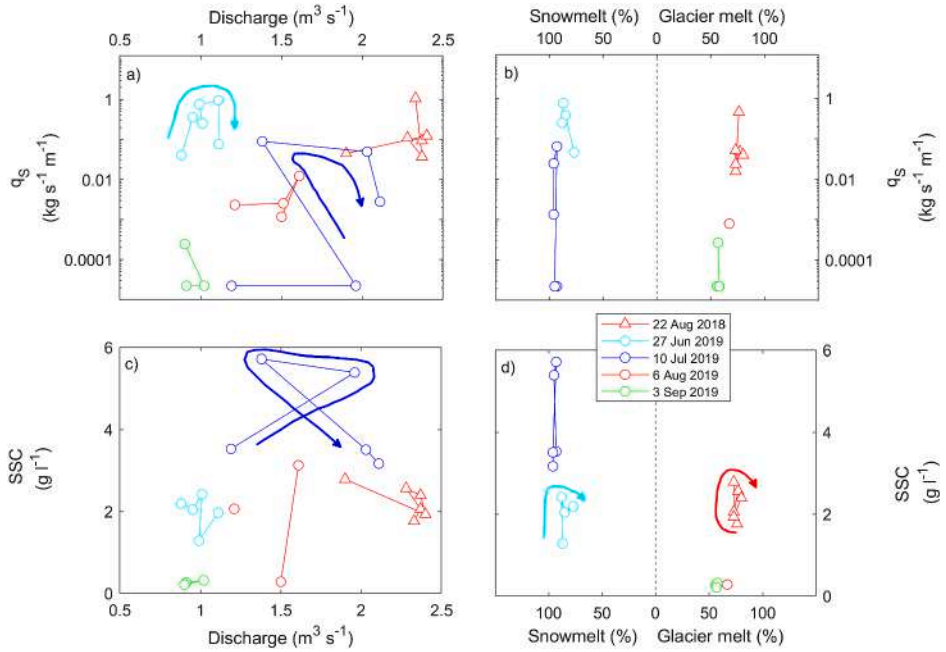

Fig. 8. Hysteresis of discharge, meltwater proportion (snowmelt and/or glacier melt %), bedload concentration, and SSC at DG on sampling days from 2017 to 2019.

Table 4
Hysteresis pattern of discharge, meltwater contributions, bedload, and SSC during melt event-based sampling at CG and DG. CW and CCW denote clockwise and counterclockwise hysteresis, respectively. – labels indicate parameter combinations without a clear hysteresis classification.

Location	Sampling day	Parameter			
		Discharge vs. bedload concentration	Glacier melt vs. bedload concentration	Discharge vs. SSC	Glacier melt vs. SSC
CG	30 Aug 2017	–	–	–	CW
	22 Aug 2018	CW	–	CW	–
	27 Jun 2019	–	–	CW	
	10 Jul 2019	–	CW	–	CCW
	24 Jul 2019	CW	–	–	–
DG	26 Jul 2018	–	–	–	–
	22 Aug 2018	–	–	–	CW
	27 Jun 2019	CW	–	–	CW
	10 Jul 2019	CW	–	eight shape	–
	6 Aug 2019	–	–	–	–
	3 Sep 2019	–	–	–	–

4. Discussion

4.1. Glacier characteristics control sediment transport

The mass balance, and consequently the runoff, of a glacier is generally determined by its size and other topographical features (Evans, 2006). In this context, the role of size, debris cover, lithology of the bedrock and elevation range (Table 1) of CG and DG will be considered in relation to the runoff and related sediment transport.

In general, the observed bedload transport and SSC tended to be higher at DG than CG (Figs. 4 and 5). First, the larger size of DG in comparison to CG naturally leads to a larger subglacial drainage area and thus higher meltwater discharge rates, which drives subglacial erosion, sediment connectivity and sediment entrainment (Hallet et al., 1996; Mao et al., 2017; Perolo et al., 2019) as long as sediment supply is sustained. While CG flows on bedrock, till deposits form the substrate located underneath the lower part of DG and thus increase sediment availability. In the case of DG, the larger sediment supply is associated with the presence of debris cover and proportion of more weatherable dolomitic rocks. This explanation may contradict the attenuating effect of the debris cover to lead to a less efficient subglacial system (Fyffe et al., 2019a), but Nicholson and Benn (2012) and Fyffe et al. (2014) found that supraglacial debris cover affected the spatial distribution of melt processes and thus increased transport of bedload and fine sediments. The debris-covered glacier also exhibits sections of basal ice, rich in sediment, exposed at ice margins. Where meltwater intersects such basal ice, high sediment loads can be expected and observed, but the distribution of the basal ice in relation to the subglacial drainage network is not easily determined. Nevertheless, the presence of this rich source of sediment is known at DG and not confirmed at CG and its availability may contribute to some of the patterns observed. While the formation of basal ice is not directly related to the presence of a debris cover, in general, it is more likely to form where the glacier system is relatively debris rich, and the glacier history shows complex interaction with pro and paraglacial sediments as is the case of DG at this site (Savi et al., submitted).

Regarding the lithology of the subglacial sediments, metamorphic rocks are present below both glaciers (Table 1). However, composition of the bedload collected indicated that bedload from DG mostly consisted of dolomitic rocks with a share of conglomerates, while bedload from CG was only metamorphic, reflecting the underlying lithology of the catchment.

Also, the smaller elevation range and lower mean elevation of DG could lead to higher sediment transport as the entire glacier body likely experiences relatively higher temperatures in the ablation zone (roughly 1.6 °C assuming a 6.5 °C/km lapse rate) with temperature-driven melting expected to occur earlier and more frequently than at CG.

Only the higher slope at CG could support increased sediment

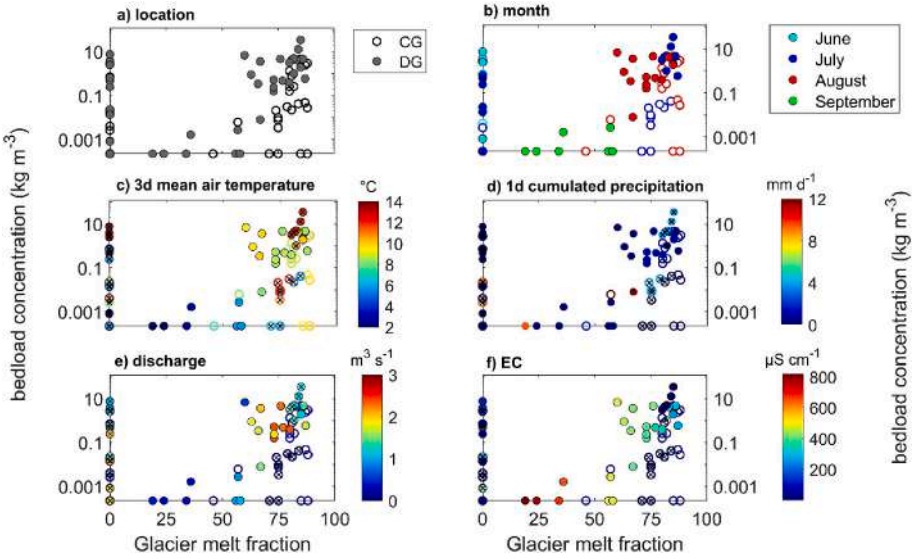

Fig. 9. Bedload concentration as a function of glacier melt fraction with respect to spatio-temporal sampling characteristics (sampling location and month), hydro-meteorological (3d mean air temperature, 1d cumulated precipitation, and discharge) and hydrochemical (EC) conditions. Meteorological parameters were measured at AWS Madritsch. Cross symbols indicate the presence of snowmelt. The color bar represents the individual range of parameter values.

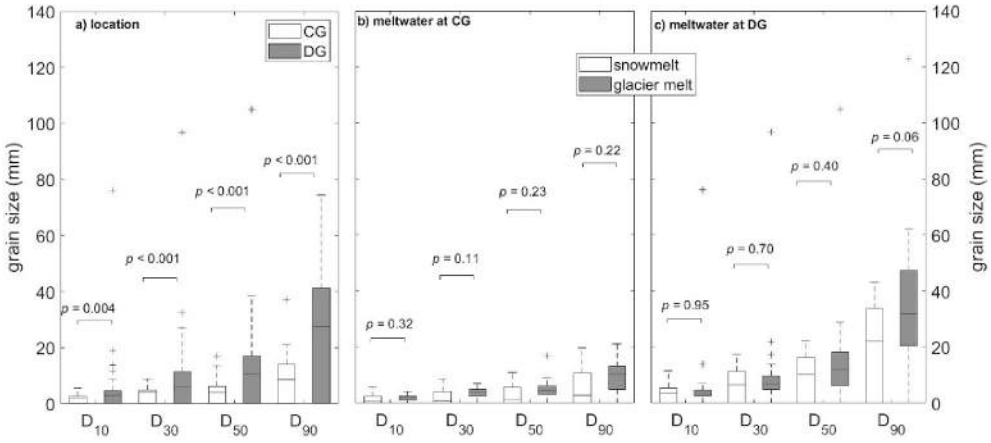

Fig. 10. Grain size distributions D10, D30, D50, and D90 at CG and DG and the dominant runoff component (snowmelt vs. glacier melt) at these glaciers. Grain size distributions were evaluated only for snowmelt or glacier melt contributions greater than 60 %. The *p*-values are derived from the Wilcoxon Rank rank sum test.

transport by higher melt rates. While the higher slope generally intensifies water velocity along the glacier bed and thus sediment transport (Delaney et al., 2018), the favourable exposure guarantees longer irradiation times and thus more radiation energy available for snow and ice melting (Hock, 2005). The effect of both drivers may be superimposed and likely compensated by the effects exhibited by glacier size, presence of debris cover, and subglacial deposits. Among all reported drivers of sediment transport in this analysis, glacier size, presence of debris cover, as well the presence/abundance of subglacial till deposits (unfortunately unknown) are most likely to dictate the hydrological and sedimentary boundary conditions of CG and DG and to explain their contrasting sediment transport. Yet, it remains challenging to generalize these controls and transfer their effects on meltwater dynamics and sediment transport to other glaciers given that each glacier has its own topoclimatic, geological and geomorphological context (Bogen, 1996; Zekollari et al., 2020; Nicholson et al., 2021).

4.2. Runoff processes determine sediment transport

As a consequence of the previously described drivers, the dynamics and magnitude of proglacial meltwater contributions at CG and DG followed the seasonal transition of meltwater composition, commonly found in glacierized catchments (Jeelani et al., 2012; Penna et al., 2017): snowmelt dominated proglacial runoff in early summer, followed by a transition phase of increasing glacier melt contributions during summer reaching its maximum at the end of summer. Because cumulated daily total precipitation was always less than 12 mm d^{-1} on the sampling and preceding day, we could not proof that rainfall was a major runoff component and potential driver of sediment transport.

In this context, the different phases of dominant runoff components guide the sensitivity of sediment transport as follows:

i) During snowmelt, bedload concentrations at CG and DG were one order of magnitude lower than during glacier melt. Although the sampling location was not proglacial and thus limiting the comparability, sediment transport was up to 6 times higher at the Matsch glacier (similar region than this study; Comiti et al., 2019) and the Estero Morales glacier, Chile (Carrillo and Mao, 2020). Mao et al. (2014) explained this observation by sediment sources being likely disconnected under snowmelt conditions.
ii) During glacier melt, bedload transport is highest and its magnitude is determined by the intensity of glacier melt (Comiti et al.,

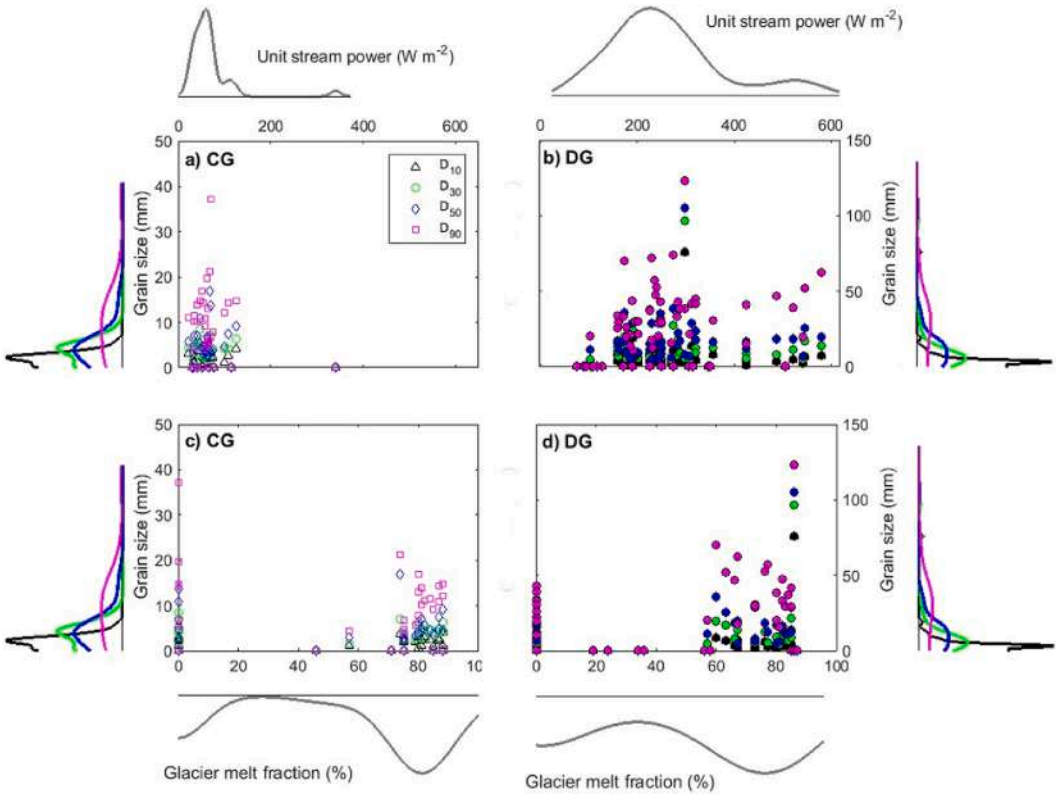

Fig. 11. Grain size distribution as a function of unit stream power and glacier melt fraction at the sampling locations CG and DG. The frequency plots show the sample distribution with respect to (a,b) unit stream power and (c,d) glacier melt fraction on the x-axis and grain size on the y-axis at both sites. The different colors represent the classes of grain size distribution D_{10}, D_{30}, D_{50}, and D_{90}.

2019; Carrillo and Mao, 2020). The observation that increasing proportions of glacier melt could mobilize bedload of larger grain sizes was also supported by Perolo et al. (2019). As the grain size may infer the diameter of subglacial conduits (Davies et al., 2003), reflecting the evolution of the subglacial drainage system (Röthlisberger and Lang, 1987), we argue that the subglacial drainage system of the larger DG developed larger conduits, becoming more effective to accommodate more meltwater and larger sediment clasts. In addition, the larger availability of sediment from the supraglacial debris cover, particularly above undercutting supraglacial streams or exposed ice cliffs, combined with the presence of erodible till deposit accessible by subglacial streams may contribute to the larger volume of bedload transport measured at DG compared to CG.

iii) Beside these typical periods of clear relationship between runoff source and bedload transport, intense periods of snowmelt, such as observed in Spring 2019, may induce bedload transport at similar orders of magnitude as during the glacier melt period. Indeed, the late, abundant snow in April and May 2019 was followed by a very hot and dry June (Savi et al., 2023). In agreement, also Carrillo and Mao (2020) observed highest bedload transport during the snowmelt period. Snowmelt can be a major driver of melting cycles (Nienow et al., 1998) so that intense snowmelt fluxes reach the poorly drained, distributed subglacial drainage area (Iken and Bindschadler, 1986; Hubbard and Nienow, 1997) that formed on the glacier during the previous year and activated non-evacuated sediment deposits from the previous melting season. This explanation may lead to the inference that sediment transport in early summer is controlled by antecedent subglacial flow conditions of the previous season, a concept which is accepted so far only for sediment entrainment at the event scale in alpine streams (Mao et al., 2017).

iv) In contrast to the melting season, the onset of baseflow conditions at DG showed almost no sediment transport, such as in September 2019 (mean SSC: 0.16 g l^{-1}; no bedload concentration) and no transport of suspended sediment and bedload at all during winter baseflow (field evidence from January 2020). Similar observations were made at Bosson glacier, France by Guillon et al. (2018) and attributed to the seasonal closing of the subglacial drainage system. Unlike SSC, daily bedload concentration minima in June and July could reach concentrations typical of baseflow conditions in September. This fact possibly indicates a daily exhaustion of bedload source that becomes activated day by day.

Considering the hydro-meteorological drivers, our observations revealed a complex and non-linear relationship between air temperatures, meltwater dynamics at the daily scale, and resulting sediment transport.

The observation of higher discharge and sediment transport during lower air temperature in July compared to June highlights that the daily subglacial discharge and sediment transport is not only determined by short-term meteorological conditions, but responds to antecedent conditions such as previous warm spells and the state of the subglacial drainage network (e.g. at CG and DG on 27 June and 10 July 2019). This interpretation is corroborated by the observation of similar discharge and sediment transport dynamics during different air temperature conditions (e.g. at CG and DG on 10 and 24 July 2019). Also in August, both discharge and sediment transport indicated individual dynamics not controlled by air temperature. Therefore, independent of the glacier type (i.e. CG and DG), hydrological and subglacial processes at the daily scale may be superimposed by weekly processes related to the evolution of the subglacial drainage system as follows: i) In early summer, the distributed subglacial drainage system progressively routes meltwater through the glacier body, and interconnects subglacial bedload and

basal sediment sources. Consequently, melt-induced runoff and sediment transport increase from June to July, despite similar daily air temperature. ii) In contrast, in July similar runoff and sediment transport under varying air temperature show that the subglacial drainage network has reached its channelized form. It follows that sediment transport dynamics are decoupled from daily air temperature. iii) Finally, in August, the channelized subglacial drainage system occupies the largest extend, but it may have variable efficiency to access basal sediment sources or the drainage area becomes exhausted, thus being responsible for individual dynamics of runoff and sediment transport.

These relationships are often non-linear (Mao et al., 2019) so that their daily dynamics may temporally not coincide and experience different evolution during the day (e.g. constant discharge accompanied with variable sediment transport at CG on 27 June, 10 and 24 July 2019).

4.3. Origin of suspended sediments and bedload

Ronald (2020) suggested that the major source of fine sediment at DG might be a sediment-rich basal ice and not the debris-cover, which is mainly composed of large rocks and a thin layer of fine sediments. Instead, bedload likely originates from subglacial sources activated during the seasonal development of the subglacial drainage system and probably also at the daily scale.

In contrast, sampled sediments at CG likely originated from subglacial till and subglacial bedrock because sediment supply is limited to only few supraglacial deposits (when rockfalls occurred and debris was laterally placed on the glacier).

Despite the contrasting availability and locations of sediment supply, clockwise hysteresis (higher transport on the rising hydrograph limb) was rarely seen for both proglacial streams and may support again the inference of daily exhaustion of sediment sources during snowmelt or temporal storage of sediments during glacier melt (Mao et al., 2014). Also, the fact that a clear hysteresis pattern could not be attributed to the majority of runoff events was the reason why the observation on the seasonal shift from clockwise to counterclockwise hysteresis could not be made (Stott et al., 2014; Carrillo and Mao, 2020). Therefore, the progressively seasonal exhaustion of sediment supply at CG and DG could not be confirmed and may instead occur at the daily scale. This observation underlines the assumption of Mao et al. (2014) that sediment-discharge hysteresis loops could be absent at the glacier mouth, where a sediment supply unlimited system prevails. Such an unlimited supply implies that most of the bedload and fine sediment sources were connected to the runoff generating areas, i.e. mainly the subglacial drainage system. From our perception, the assumption of Comiti et al. (2019) about a progressive shift from supply-limited (driven by glacier activity) to transport-limited (during rainfall-induced events) sediment transport may not fully apply for CG and DG because the boundary conditions in the present catchment are different. For example, additional specifications (such as distance to the glacier, geology of the catchment) may be required to valid the assumption also in the proglacial environment underlain by sedimentary rocks.

4.4. Implications for hydrology and sediment transport at CG and DG

This study was carried out about 30 years after the last maximum advance stage of the glaciers in the Sulden valley (Savi et al., 2021b) and corresponds to the phase of declining discharge after the “peak water” stage of maximum annual discharge (Carturan et al., 2019). In future, climate warming could anticipate the maximum seasonal discharge, which may shift from July and August to earlier months in the year (Raymond Pralong et al., 2015). Simultaneously, the development of the subglacial drainage system and the seasonal glacier melt peak may shift earlier in the season. Due to the strong relationship between glacier melt and sediment transport as observed in this study, the release of bedload and suspended sediments will likely follow this trend.

Warming will also raise the equilibrium line altitude to higher elevations (Beniston, 2003; Huss and Hock, 2015; Knoll and Kerschner, 2010), so that the ablation zone and the subglacial drainage system will likely extend and rise in altitude (Gagliardini and Werder, 2018). Meltwater could then activate new till reservoirs, which were not previously exposed to high water velocities to allow entrainment (Delaney and Adhikari, 2020).

In turn, losses of ice masses will lead to decreasing glacier melt, initiating a transition of melt-induced to rainfall-induced sediment transport (Buter et al., 2022). Consequently, sediment activation could be controlled by periglacial instead of subglacial processes (Guillon et al., 2015; Savi et al., submitted). Although rain events did not play a dominant role on runoff generation during this study, it is possible that daily variations of sediment transport could become much larger, particularly under more intense rain events (Coviello et al., 2022). At the daily scale, the dynamics of bedload and SSC showed non-linear behaviour in relation to air temperature, likely resulting in a more complex interplay of meltwater (glacier melt, in particular) and sediment transport due to higher daily air temperatures.

Against this background, despite speculation, we attempt to characterize the further development of the meltwater and sediment transport pattern at CG and DG. Representing a clean-ice glacier, CG will further continue to retreat reaching mass balance equilibrium under current climate conditions (Scherler et al., 2011). Few supraglacial sediments from lateral rockfalls could locally enhance ablation and promote the glacier margin to retreat faster (Fyffe et al., 2019b). Such continuous glacier retreat over several years will probably alter the hydraulic gradients, leading to higher subglacial water velocities independently of the meltwater discharge (Delaney et al., 2019) and thus increasing sediment transport. We can only speculate on the extent of subglacial till reservoirs of CG, but controls of sediment transport will presumably change from subglacial to periglacial processes (Guillon et al., 2015).

As an example of a debris-covered glacier, DG will likely become thinner at the lower tongue but may experience a slower and not uniform frontal retreat in contrast to CG (Savi et al., 2021b). The debris cover will likely be supplied by enhanced rockfalls from the bedrock walls surrounding the glacier, induced by thawing permafrost (e.g. Gruber et al., 2004) and frost-cracking activity (e.g. Savi et al., 2021a). Under these conditions, DG will further be prevented from achieving a steady state of glacier mass balance with current climate conditions (Nicholson et al., 2021). Although the work of Ronald (2020) gave first insights into the extent of the subglacial drainage system and the importance of basal ice as a source of fine sediments, knowledge of the amount and location of subglacial till deposits and the bedrock morphology remains unknown and will require further research to better quantify future sediment supply at DG.

5. Conclusions

The present study was conducted to relate the runoff composition and meltwater dynamics at two proglacial streams to sediment transport, to analyse the temporal and spatial variability of this relationship, and to assess the sensitivity of meteorological conditions and glacier characteristics as potential drivers. Our results show that:

- Using $\delta^{18}O$ and EC, the hydrochemical characterization revealed snowmelt and glacier melt as dominant runoff components at CG and DG. The highest proglacial water discharges of up to 2.4 m^3/s at DG were composed of 73 % of glacier melt and minor proportions of snowmelt (up to 27 %). In contrast, the highest glacier melt contributions of 87 % were estimated for intermediate discharge of 1.68 m^3/s.
- At the seasonal scale, bedload concentrations and SSC at CG and DG strongly varied similarly to the discharge variations. Large daily variations of up to two orders of magnitude made the seasonal

development of bedload concentrations at CG and DG less clear. SSC at both sites showed large monthly variations of three orders of magnitude at DG and only one order of magnitude at CG.

- At the daily scale, increasing discharge generally controlled the dynamics of bedload and SSC, but an added complexity could be inferred as i) discharge and sediment transport did not always follow the daily variation of air temperature by a clear rising and falling limb, and ii) similar daily air temperatures resulted in different discharge and sediment transport responses and vice versa. Daily exhaustion of bedload sediment sources at DG were inferred from the fact that daily bedload concentration minima in June and July at DG were similar to concentrations during baseflow conditions in September.
- The sensitivity of glacier melt regarding meteorological conditions showed that highest glacier melt occurred when weekly mean air temperature were above 8 °C and only little precipitation fell. Low to medium glacier melt contributions (19 to 58 %) at CG and DG were associated with relatively low bedload concentrations of up to 0.001 kg m^{-3}, whereas 75 to 80 % of glacier melt led to bedload concentrations of 1 to 10 kg m^{-3} at DG and much lower concentrations of 0.01 to 1 kg m^{-3} at CG.

The findings confirm the initial hypothesis that contrasting features of DG and CG are drivers of contrasting meltwater dynamics and sediment transport. More specifically, glacier size, presence of debris cover, and the abundance of subglacial till most likely dictate the hydrological and sedimentary boundary conditions of CG and DG and explain their contrasting sediment transport characteristics. However, generalizing these controls and transferring their effects on meltwater dynamics and sediment transport to other glaciers is a research gap to be addressed in future studies.

Finally, our study adds further insights into the interplay of meltwater contributions and sediment transport and its spatial and temporal dynamics at the event and seasonal scale. It thus represents an important contribution to better assess the impact of climate warming in glacierized catchments.

CRediT authorship contribution statement

Michael Engel: Writing – original draft, Investigation, Formal analysis, Data curation, Conceptualization. **Velio Coviello:** Writing – review & editing, Investigation. **Sara Savi:** Investigation, Writing – review & editing. **Anuschka Buter:** Investigation. **Andrea Andreoli:** Writing – review & editing, Investigation. **Shusuke Miyata:** Investigation, Writing – review & editing. **Giulia Marchetti:** Investigation, Writing – review & editing. **Vittoria Scorpio:** Investigation, Writing – review & editing. **Sara Rathburn:** Investigation, Writing – review & editing. **Lindsey Nicholson:** Investigation, Writing – review & editing. **Francesco Comiti:** Conceptualization, Funding acquisition, Project administration, Writing – review & editing.

Declaration of competing interest

The authors declare that they have no known competing financial interests or personal relationships that could have appeared to influence the work reported in this paper.

Data availability

Data will be made available on request.

Acknowledgments

This research was funded by the project GLORI (Glaciers-To-Rivers Sediment Transfer In Alpine Basins) granted by the Autonomous Province of Bozen-Bolzano and by the project SEDIPLAN-r, funded by the EU FESR/EFRE program.

The authors thank Christian Grumer and Ricardo Carillo for their field assistance. A special thanks goes to Velio Coviello, who was – beside a real friend – an excellent, open-minded researcher that made possible this work with his passion and great enthusiasm for field work.

We thank the Hydrographic Office and the Department of Hydraulic Engineering of the Autonomous Province of Bozen-Bolzano for providing meteorological and hydrometric data. We acknowledge the Forestry Commission Office Prat, the National Park Stilfserjoch (Passo Stelvio), and the cable car Sulden GmbH for their logistical support and helpful advice.

Appendix A. Supplementary data

Supplementary data to this article can be found online at https://doi.org/10.1016/j.jhydrol.2024.131171.

References

Antoniazza, G., Nicollier, T., Boss, S., Mettra, F., Badoux, A., Schaefli, B., Rickenmann, D., Lane, S.N., 2022. Hydrological drivers of bedload transport in an alpine watershed. Water Resour. Res. 58 https://doi.org/10.1029/2021WR030663.

Arnoldi, 2021. Seismic monitoring of bedload transport in a proglacial stream (Sulden/Solda River, Italian Alps). Master Thesis in Environmental Management of Mountain Areas, Free University of Bozen/Bolzano and University of Innsbruck.

Ayala, A., Pellicciotti, F., MacDonell, S., McPhee, J., Vivero, S., Campos, C., Egli, P., 2016. Modelling the hydrological response of debris-free and debris-covered glaciers to present climatic conditions in the semiarid Andes of central Chile. Hydrol. Process. 30, 4036–4058. https://doi.org/10.1002/hyp.10971.

Beniston, M., 2003. Climatic change in mountain regions: a review of possible impacts. Clim. Change 59, 5–31. https://doi.org/10.1023/A: 1024458411589.

Beniston, M., Farinotti, D., Stoffel, M., Andreassen, L.M., Coppola, E., Eckert, N., Fantini, A., Giacona, F., Hauck, C., Huss, M., Huwald, H., Lehning, M., López-Moreno, J.-I., Magnusson, J., Marty, C., Morán-Tejéda, E., Morin, S., Naaim, M., Provenzale, A., Rabatel, A., Six, D., Stötter, J., Strasser, U., Terzago, S., Vincent, C., 2018. The European mountain cryosphere: a review of its current state, trends, and future challenges. Cryosph. 12, 759–794. https://doi.org/10.5194/tc-12-759-2018.

Beniston, M., Stoffel, M., 2014. Assessing the impacts of climatic change on mountain water resources. Sci. Total Environ. 493, 1129–1137. https://doi.org/10.1016/j.scitotenv.2013.11.122.

Boeckli, L., Brenning, A., Gruber, S., Noetzli, J., 2012. A statistical approach to modelling permafrost distribution in the European Alps or similar mountain ranges. Cryosph. 6, 125–140. https://doi.org/10.5194/tc-6-125-2012.

Bogen, J., 1996. Erosion rates and sediment yields of glaciers.pdf. Ann. Glaciol. 22.

Brighenti, S., Tolotti, M., Bruno, M.C., Engel, M., Wharton, G., Cerasino, L., Mair, V., Bertoldi, W., 2019. After the peak water: the increasing influence of rock glaciers on alpine river systems. Hydrol. Process. 33, 2804–2823. https://doi.org/10.1002/hyp.13533.

Bunte, K., Abt, S.R., Potyondy, J.P., Ryan, S.E., 2004. Measurement of coarse gravel and cobble transport using a portable bedload trap. J. Hydraul. Eng. 130 (9), 879–893.

Buter, A., Spitzer, A., Comiti, F., Heckmann, T., 2020. Geomorphology of the Sulden River basin (Italian Alps) with a focus on sediment connectivity. J. Maps 16, 890–901. https://doi.org/10.1080/17445647.2020.1841036.

Buter, A., Heckmann, T., Filisetti, L., Savi, S., Mao, L., Gems, B., Comiti, F., 2022. Effects of catchment characteristics and hydro-meteorological scenarios on sediment connectivity in glacierised catchments. Geomorphology 402, 108128. https://doi.org/10.1016/j.geomorph.2022.108128.

Carrillo, R., Mao, L., 2020. Coupling sediment transport dynamics with sediment and discharge sources in a glacial andean basin. Water (switzerland) 12, 1–25. https://doi.org/10.3390/w12123452.

Carrivick, J.L., Heckmann, T., 2017. Short-term geomorphological evolution of proglacial systems. Geomorphology 287, 3–28. https://doi.org/10.1016/j.geomorph. 2017.01.037.

Carturan, L., De Blasi, F., Cazorzi, F., Zoccatelli, D., Bonato, P., Borga, M., Dalla Fontana, G., 2019. Relevance and scale dependence of hydrological changes in glacierized catchments: Insights from historical data series in the Eastern Italian Alps. Water (Switzerland) 11. https://doi.org/10.3390/w11010089.

Christopherson, N., Hooper, R.P., 1992. Multivariate analysis of stream water chemical data: the use of principal component analysis for the endmember mixing problem. Water Resour. Res. 28, 99–107.

Collins, D.N., 1989. Seasonal development of subglacial drainage and suspended sediment delivery to melt waters beneath an alpine glacier. Ann. Glaciol. 13, 45–50. https://doi.org/10.1017/s026030550000762x.

Comiti, F., Mao, L., Penna, D., Dell'Agnese, A., Engel, M., Rathburn, S., Cavalli, M., 2019. Glacier melt runoff controls bedload transport in Alpine catchments. Earth Planet. Sci. Lett. 520, 77–86. https://doi.org/10.1016/j.epsl.2019.05.031.

Cook, S.J., Swift, D.A., 2012. Subglacial basins: Their origin and importance in glacial systems and landscapes. Earth-Science Rev. 115, 332–372. https://doi.org/10.1016/j.earscirev.2012.09.009.

Coviello, V., Vignoli, G., Simoni, S., Bertoldi, W., Engel, M., Buter, A., Marchetti, G., Andreoli, A., Savi, S., Comiti, F., 2022. Bedload fluxes in a glacier-fed river at multiple temporal scales. Earth Sp. Sci. Open Arch. 27.
Davies, T.R.H., Smart, C.C., Turnbull, J.M., 2003. Water and sediment outbursts from advanced Franz Jozef Glacier, New Zealand. Earth Surf. Process. Landforms 28, 1081–1096. https://doi.org/10.1002/esp.515.
Delaney, I., Adhikari, S., 2020. Increased subglacial sediment discharge in a warming climate: consideration of ice dynamics, glacial erosion, and fluvial sediment transport. Geophys. Res. Lett. 47, 1–11. https://doi.org/10.1029/2019GL085672.
Delaney, I., Bauder, A., Werder, M.A., Farinotti, D., 2018. Regional and annual variability in subglacial sediment transport by water for two glaciers in the Swiss alps. Front. Earth Sci. 6, 1–17. https://doi.org/10.3389/feart.2018.00175.
Delaney, I., Werder, M.A., Farinotti, D., 2019. A Numerical Model for Fluvial Transport of Subglacial Sediment. J. Geophys. Res. Earth Surf. 124, 2197–2223. https://doi.org/10.1029/2019JF005004.
Dell'Agnese, A., Mao, L., Comiti, F., 2014. Calibration of an acoustic pipe sensor through bedload traps in a glacierized basin. Catena 121, 222–231. https://doi.org/10.1016/j.catena.2014.05.021.
Duethmann, D., Bolch, T., Farinotti, D., Kriegel, D., Vorogushyn, S., Merz, B., Pieczonka, T., Jiang, T., Su, B., Güntner, A., 2015. Attribution of streamflow trends in snow and glacier melt-dominated catchments of the Tarim River. Central Asia. Water Resour. Res. 51, 4727–4750. https://doi.org/10.1002/2014WR016716.
Engel, M., Penna, D., Bertoldi, G., Dell'Agnese, A., Soulsby, C., Comiti, F., 2016. Identifying run-off contributions during melt-induced runoff events in a glacierized Alpine catchment. Hydrol. Process. 30, 343–364. https://doi.org/10.1002/hyp.10577.
Engel, M., Penna, D., Bertoldi, G., Vignoli, G., Tirler, W., Comiti, F., 2018. Controls on spatial and temporal variability of streamflow and hydrochemistry in a glacierized catchment. Hydrol. Earth Syst. Sci. 23, 2041–2063. https://doi.org/10.5194/hess-23-2041-2019.
Evans, I.S., 2006. Glacier distribution in the alps: statistical modelling of altitude and aspect. Geogr. Ann. 88 A, 115–133.
Fyffe, C.L., Reid, T.D., Brock, B.W., Kirkbride, M.P., Diolaiuti, G., Smiraglia, C., Diotri, F., 2014. A distributed energy-balance melt model of an alpine debris-covered glacier. J. Glaciol. 60 (221), 587–602.
Fyffe, C.L., Brock, B.W., Kirkbride, M.P., Black, A.R., Smiraglia, C., Diolaiuti, G., 2019a. The impact of supraglacial debris on proglacial runoff and water chemistry. J. Hydrol. 576, 41–57. https://doi.org/10.1016/j.jhydrol.2019.06.023.
Fyffe, C.L., Brock, B.W., Kirkbride, M.P., Mair, D.W.F., Arnold, N.S., Smiraglia, C., Diolaiuti, G., Diotri, F., 2019b. Do debris-covered glaciers demonstrate distinctive hydrological behaviour compared to clean glaciers? J. Hydrol. 570, 584–597. https://doi.org/10.1016/j.jhydrol.2018.12.069.
Gagliardini, O., Werder, M.A., 2018. Influence of increasing surface melt over decadal timescales on land-terminating Greenland-type outlet glaciers. J. Glaciol. 64, 700–710. https://doi.org/10.1017/jog.2018.59.
Galos, S.P., Klug, C., Prinz, R., Rieg, L., Sailer, R., Dinale, R., Kaser, G., 2015. Recent glacier changes and related contribution potential to river discharge in the Vinschgau / Val Venosta, Italian Alps. Geogr. Fis. e Din. Quat. 38, 143–154. https://doi.org/10.4461/GFDQ.2015.38.13.
Genereux, D., 1998. Quantifying uncertainty in tracer-based hydrograph separations, Water Resour. Res. 34, 915–919. https://doi.org/10.1029/98WR00010.
Gobiet, A., Kotlarski, S., Beniston, M., Heinrich, G., Rajczak, J., Stoffel, M., 2014. 21st century climate change in the European Alps-A review. Sci. Total Environ. 493, 1138–1151. https://doi.org/10.1016/j.scitotenv.2013.07.050.
Gröning, M., Lutz, H.O., Roller-Lutz, Z., Kralik, M., Gourcy, L., Pöltenstein, L., 2012. A simple rain collector preventing water re-evaporation dedicated for δ18O and δ2H analysis of cumulative precipitation samples. Journal of Hydrology 448–449, 195–200. https://doi.org/10.1016/j.jhydrol.2012.04.041.
Gruber, S., Hoelzle, M., Haeberli, W., 2004. Permafrost thaw and destabilization of Alpine rock walls in the hot summer of 2003. Geophys. Res. Lett. 31, 1–4. https://doi.org/10.1029/2004GL020051.
Guillon, H., Mugnier, J.L., Buoncristiani, J.F., Carcaillet, J., Godon, C., Prud'homme, C., vander Beek, P., Vassallo, R., 2015. Improved discrimination of subglacial and periglacial erosion using 10Be concentration measurements in subglacial and supraglacial sediment load of the Bossons glacier (Mont Blanc massif, France). Earth Surf. Process. Landforms 40, 1202–1215. https://doi.org/10.1002/esp.3713.
Guillon, H., Mugnier, J.L., Buoncristiani, J.F., 2018. Proglacial sediment dynamics from daily to seasonal scales in a glaciated Alpine catchment (Bossons glacier, Mont Blanc massif, France). Earth Surf. Process. Landforms 43, 1478–1495. https://doi.org/10.1002/esp.4333.
Gurnell, A., Hannah, D., Lawler, D.,1996. Suspended sediment yield from glacier basins. In: Walling, D.E. & Webb, B.W. (Eds.), Erosion and Sediment Yield: Global and Regional Perspectives, Vol. 236. International Association of Hydrological Sciences Publication, pp. 97–104. http://hydrologie.org/redbooks/a236/iahs_236_0097.pdf.
Hallet, B., Hunter, L., Bogen, J., 1996. Rates of erosion and sediment evacuation by glaciers: A review of field data and their implications. Global and Planetary Change 12, 213–235.
Haritashya, U.K., Singh, P., Kumar, N., Gupta, R.P., 2006. Suspended sediment from the Gangotri Glacier: Quantification, variability and associations with discharge and air temperature. J. Hydrol. 321, 116–130. https://doi.org/10.1016/j.jhydrol.2005.07.037.
Hasnain, S.I., Thayyen, R.J., 1999. Discharge and suspended-sediment concentration of meltwaters, draining from the Dokriani glacier, Garhwal Himalaya. India. J. Hydrol. 218, 191–198. https://doi.org/10.1016/S0022-1694(99)00033-5.
Heckmann, T., Schwanghart, W., 2013. Geomorphic coupling and sediment connectivity in an alpine catchment – Exploring sediment cascades using graph theory. Geomorphology 182, 89–103. https://doi.org/10.1016/j.geomorph.2012.10.033.
Hock, R., 2005. Glacier melt: a review of processes and their modelling. Prog. Phys. Geogr. 29, 362–391. https://doi.org/10.1191/0309133305 pp453ra.
Hubbard, B., Nienow, P.W., 1997. Alpine subglacial hydrology. Quat. Sci. Rev. 16, 939–955.
Huss, M., Hock, R., 2015. A new model for global glacier change and sea-level rise. Front. Earth Sci. 3, 1–22. https://doi.org/10.3389/feart.2015.00054.
Huss, M., Hock, R., 2018. Global-scale hydrological response to future glacier mass loss. Nat. Clim. Chang. 8, 135–140. https://doi.org/10.1038/s41558-017-0049-x.
Iken, A., Bindschadler, R.A., 1986. Combined measurements of Subglacial Water Pressure and Surface Velocity of Findelengletscher, Switzerland: Conclusions about Drainage System and Sliding Mechanism. J. Glaciol. 32, 101–119. https://doi.org/10.3189/s0022143000006936.
Jeelani, G., Feddema, J.J., Veen, C.J. Van Der, Stearns, L., 2012. Role of snow and glacier melt in controlling river hydrology in Liddar watershed (western Himalaya) under current and future climate. Water Resour. Res. 48, 1–16. https://doi.org/10.1029/2011WR011590.
Klaus, J., McDonnell, J.J., 2013. Hydrograph separation using stable isotopes: Review and evaluation. J. Hydrol. 505, 47–64. https://doi.org/10.1016/j.jhydrol.2013.09.006.
Knoll, C., Kerschner, H., 2010. A glacier inventory for South Tyrol, Italy, based on airborne laser-scanner data. Ann. Glaciol. 50, 46–52.
Lane, S.N., Bakker, M., Gabbud, C., Micheletti, N., Saugy, J.N., 2017. Sediment export, transient landscape response and catchment-scale connectivity following rapid climate warming and Alpine glacier recession. Geomorphology 277, 210–227. https://doi.org/10.1016/j.geomorph.2016.02.015.
Mao, L., Dell'Agnese, A., Huincache, C., Penna, D., Engel, M., Niedrist, G., Comiti, F., 2014. Bedload hysteresis in a glacier-fed mountain river. Earth Surf. Process. Landforms 39, 964–976. https://doi.org/10.1002/esp.3563.
Mao, L., Dell'Agnese, A., Comiti, F., 2017. Sediment motion and velocity in a glacier-fed stream. Geomorphology 291, 69–79. https://doi.org/10.1016/j.geomorph.2016.09.008.
Mao, L., Comiti, F., Carrillo, R., Penna, D., 2019. Sediment Transport in Proglacial Rivers, in: Heckmann, T., Morche, D. (Eds.). pp. 199–217. https://doi.org/10.1007/978-3-319-94184-4_12.
Micheletti, N., Lane, S.N., 2016. Water yield and sediment export in small, partially glaciated Alpine watersheds in a warming climate, Water Resour. Res. 52, 4924–4943. https://doi:10.1002/2016WR018774.
Miller, J.D., Immerzeel, W.W., Rees, G., 2012. Climate Change Impacts on Glacier Hydrology and River Discharge in the Hindu Kush – Himalayas. Mt. Res. Dev. 32, 461–467.
Nicholson, L.I., Benn, D.I., 2012. Properties of natural supraglacial debris in relation to modelling sub-debris ice ablation, Earth Surf. Proc. Land. 38, 409–501. https://doi.org/10.1002/esp.3299.
Nicholson, L., Boxall, K., 2020. Supraglacial debris thickness measurements from excavation pits at Suldenferner. Zenodo.
Nicholson, L., Wirbel, A., Mayer, C., Lambrecht, A., 2021. The Challenge of Non-Stationary Feedbacks in Modeling the Response of Debris-Covered Glaciers to Climate Forcing. Front. Earth Sci. 9, 1–18. https://doi.org/10.3389/feart.2021.662695.
Nienow, P., Sharp, M., Willis, I., 1998. Seasonal changes in the morphology of the subglacial drainage system, Haut Glacier d'Arolla. Switzerland. Earth Surface Processes and Landforms 23 (9), 825–843.
Pearce, J.T., Pazzaglia, F.J., Evenson, E.B., Lawson, D.E., Alley, R.B., Germanoski, D., Denner, J.D., 2003. Bedload component of glacially discharged sediment: Insights from the Matanuska Glacier, Alaska. Geology 31, 7–10. https://doi.org/10.1130/0091-7613(2003)031<0007:BCOGDS>2.0.CO;2.
Penna, D., Engel, M., Bertoldi, G., Comiti, F., 2017. Towards a tracer-based conceptualization of meltwater dynamics and streamflow response in a glacierized catchment. Hydrol. Earth Syst. Sci. 21, 23–41. https://doi.org/10.5194/hess-21-23-2017.
Perolo, P., Bakker, M., Gabbud, C., Moradi, G., Rennie, C., Lane, S.N., 2019. Subglacial sediment production and snout marginal ice uplift during the late ablation season of a temperate valley glacier. Earth Surf. Process. Landforms 44, 1117–1136. https://doi.org/10.1002/esp.4562.
Rabanser, M., 2019. Processes of lateral moraine formation at a debris - covered glacier , Suldenferner (Vedretta di Solda), Italy 556.
Raymond Pralong, M., Turowski, J.M., Rickenmann, D., Zappa, M., 2015. Climate change impacts on bedload transport in alpine drainage basins with hydropower exploitation. Earth Surf. Process. Landforms 40, 1587–1599. https://doi.org/10.1002/esp.3737.
Ronald, C., 2020. Glacier meltwater drainage patterns, discharge and connection to sediment load at the debris-covered Suldenferner, Ortler massif, Italy , revealed through dye tracing.
Röthlisberger, H., Lang, H., 1987. Glacial hydrology. In A. M. Gurnell & M. J. Clark (eds.): Glacio-fluvial Sediment Transfer: An Alpine Perspective, 37–44. John Wiley, Chichester.
Savi, S., Comiti, F., Strecker, M.R., 2021a. Pronounced increase in slope instability linked to global warming: A case study from the eastern European Alps. Earth Surf. Process. Landforms 46, 1328–1347. https://doi.org/10.1002/esp.5100.
Savi, S., Dinale, R., Comiti, F., 2021b. The Sulden/Solda Glacier (Eastern Italian Alps): Fluctuations, Dynamics, and Topographic Control over the last 200 years. Geogr. Fis. Dinam. Quat. 44, 15–30. https://doi.org/10.4461/GFDQ.2021.44.2.

Savi, S., Buter, A., Heckmann, T., Theule, J., Mao, L., Comiti, F., 2023. Multi-temporal analysis of morphological changes in an Alpine proglacial area and their effect on sediment transfer. Catena 220, 106701. https://doi.org/10.1016/j.catena.2022.106701.

Savi, S., Pitscheider; F., Engel, M., Coviello, V., Strecker, M.R., Comiti, F., Sediment export from an Alpine proglacial area under a changing climate: budgets, rates, and geomorphological processes. Submitted to Geomorphology.

Scherler, D., Bookhagen, B., Strecker, M.R., 2011. Spatially variable response of Himalayan glaciers to climate change affected by debris cover. Nat. Geosci. 4, 156–159. https://doi.org/10.1038/ngeo1068.

Sklash, M.G., Farvolden, R.N., 1979. The role of groundwater in storm runoff. J. Hydrol. 43, 45–65.

Stott, T., Nuttall, A.-M., Biggs, E., 2014. Observed run-off and suspended sediment dynamics from a minor glacierized basin in south-west Greenland. Geografisk Tidsskrift-Danish. J. Geogr. 114 (2), 1–16. https://doi.org/10.1080/00167223.2013.862911.

Swift, D.A., Nienow, P.W., Hoey, T.B., 2005. Basal sediment evacuation by subglacial meltwater: suspended sediment transport from Haut Glacier d'Arolla, Switzerland. Earth Surf. Process. Landforms 30, 867–883. https://doi.org/10.1002/esp.1197.

Zekollari, H., Huss, M., Farinotti, D., 2020. On the Imbalance and Response Time of Glaciers in the European Alps. Geophys. Res. Lett. 47, 1–9. https://doi.org/10.1029/2019GL085578.